European Journal of Medicinal Chemistry 178 (2019) 380–389

Contents lists available at ScienceDirect

European Journal of Medicinal Chemistry

journal homepage: http://www.elsevier.com/locate/ejmech

Research paper

Exploiting the 1-(4-fluorobenzyl)piperazine fragment for the development of novel tyrosinase inhibitors as anti-melanogenic agents: Design, synthesis, structural insights and biological profile

Laura Ielo [a], Batel Deri [b], Maria Paola Germanò [a], Serena Vittorio [a], Salvatore Mirabile [a], Rosaria Gitto [a], Antonio Rapisarda [a], Simone Ronsisvalle [c], Sonia Floris [d], Yael Pazy [e], Antonella Fais [d], Ayelet Fishman [b], Laura De Luca [a, *]

[a] Department of Chemical, Biological, Pharmaceutical, and Environmental Sciences, Polo Universitario SS. Annunziata, University of Messina, Viale Palatucci 13, I-98168, Messina, Italy
[b] Department of Biotechnology and Food Engineering, Technion-Israel Institute of Technology, Haifa, 3200003, Israel
[c] Department of Drug Science, Medicinal Chemistry Section University of Catania, Catania, Italy
[d] Department of Life and Environment Sciences, University of Cagliari, I-09042, Monserrato, Cagliari, Italy
[e] Technion Center for Structural Biology, Technion-Israel Institute of Technology, Haifa, 3200003, Israel

ARTICLE INFO

Article history:
Received 12 April 2019
Received in revised form
5 June 2019
Accepted 5 June 2019
Available online 6 June 2019

Keywords:
Tyrosinase inhibitors
X-ray crystallography
Docking studies
anti-melanogenic effects
B16F10 melanoma cells

ABSTRACT

The development of Tyrosinase inhibitors (TYRIs) could represent an efficacious strategy for pharmacological intervention on skin pathologies related to aberrant production of melanin. Based on *in silico* studies we designed and tested a library of twenty-four compounds bearing the 4-(4-fluorobenzyl) piperazin-1-yl]-fragment. As result, we identified several compounds with excellent inhibit effects at low micromolar concentration against TYR from *Agaricus bisporus* (TyM). Among them, compound **25** ($IC_{50} = 0.96\ \mu M$) proved to be ~20-fold more potent than the reference compound kojic acid ($IC_{50} = 17.76\ \mu M$) having wide applications in the cosmetics and pharmaceutical industries. The mode of interaction of active inhibitor **25** was deciphered by means of crystallography as well as molecular docking and these results were consistent with kinetic experiments. Moreover, the identified compound **25** exhibited no considerable cytotoxicity and showed anti-melanogenic effects on B16F10 melanoma cells. Therefore, a combination of computational and biochemical approaches could represent a rational guidelines for further structural modification of this class of compounds as future anti-melanogenic agents.

1. Introduction

Tyrosinases (TYRs, EC 1.14.18.1) are largely distributed enzymes in bacteria, fungi, insects, plants, and mammalians. TYR is the key enzyme that catalyzes the conversion of the substrate tyrosine into the intermediate product *o*-quinone (dopaquinone), which is further oxidized into eumelanin and pheomelanin through other interrelated enzymatic and non-enzymatic reactions [1].

In humans, melanin is responsible for absorbing light in order to protect skin cells from UVB-radiation damage. However, the aberrant production and accumulation of melanin in the face and neck usually cause common pigmentary disorders, such as melasma and post-inflammatory hyperpigmentation, and pose a serious aesthetic problem [2].

TYR inhibition is one strategy aimed at controlling the production of melanin; therefore, the development of TYR inhibitors (TYRIs) has gained high interest in the therapies of skin pathologies as well as in dermocosmetic treatments. Several well-known TYRIs as hydroquinone, arbutin, kojic acid, ascorbic acid (see Chart 1) and other molecules from natural sources are anti-melanin and whitening agents, but they have been reported to be problematic due to various adverse side effects, such as contact dermatitis, irritation, leukoderma, hypochromia, and ochronosis [2–6].

Abbreviations: TYRIs, Tyrosinase inhibitors; TyM, Agaricus bisporus; TYRIs, TYR inhibitors; TyBm, Bacillus megaterium; PAINS, pan-assay interference compounds.

* Corresponding author. Chemical, Biological, Pharmaceutical, and Environmental Sciences, (CHIBIOFARAM), University of Messina, Viale Palatucci 13, I-98168, Messina, Italy.
E-mail address: ldeluca@unime.it (L. De Luca).

https://doi.org/10.1016/j.ejmech.2019.06.019
0223-5234/

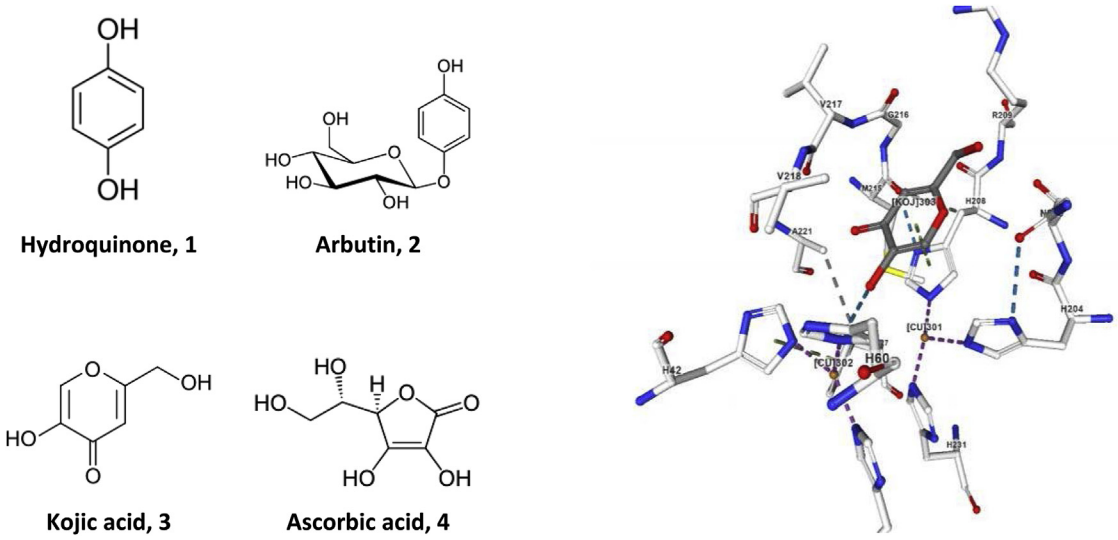

Chart 1. Chemical structures of representative TYRIs (**1**–**4**) and binding mode of kojic acid (**1**) in complex with TYR from *Bacillus megaterium* (PDB: 5I38 [8]).

The various TYRs from different species are type-3 metalloenzymes with a conserved catalytic domain, which comprises six histidine residues and two copper ions (CuA and CuB) [7] as demonstrated by X-ray structures from *Bacillus megaterium* (PDB: 5I38) [8] (see Chart 1), *Streptomyces castaneoglobisporus* (PDB: 5Z0D), *Aspegilus oryzae* (PDB: 3W6W), *Agaricus bisporus* (PDB: 2Y9X [9], and *Juglans regia* (PDB: 5CE9) [10].

Based on a combination of crystallographic and docking studies on TYRs from *Bacillus megaterium* (TyBm) and TyM, we have previously designed a new class of TYRIs that proved to be more effective than the well-known inhibitor kojic acid (**1**, KA) [11–13]. Among them, the 4-(4-fluorobenzyl)piperazin-1-yl]phenylmethanone (**5a**) and 4-(4-fluorobenzyl)piperazin-1-yl](2-methylphenyl)methanone (**5b**) (see Chart 2) displayed inhibitory effects at low micromolar concentrations toward TyM [13].

The ligand-enzyme binding profile of the best active compound **5b** (IC_{50} value of 5.25 μM) has been explored by means of theoretical and experimental studies [13]. In more detail, Fig. 1 (panel A) shows the docking pose of compound **5b** (magenta) [13] in the active site of TyM (PDB: 2Y9X). Whereas, panel B describes the binding mode of the same compound **5b** (yellow) in complex with TyBm as obtained from the crystal structure (PDB: 5OAE) [13]. These combined results highlighted the ability of inhibitor **5b** to occupy both active sites of TyM and TyBm. The 4-fluorobenzyl moiety is positioned towards the Cu ions and the oxygen of the amide group is oriented towards Arg268 in TyM or Arg209 in TyBm. Instead, the 2-methylphenyl moiety appears to be directed to the top area of the catalytic cavity of the two studied TYRs.

As continuation of this study we chose to better understand the molecular determinant controlling the interactions in the top region of the cavity for this series of 4-(4-fluorobenzyl)piperazine-derivatives (*e.g.* **5a** and **5b**). To this end, we carried out a computational approach aimed at selecting suitable substituents for decorating the aroyl moiety linked to the piperazine central core. Then, we synthesized the designed compounds, which were screened in biological assays. The most promising inhibitor was crystallized in complex with TyBm.

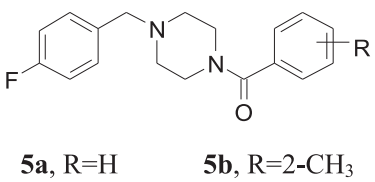

Chart 2. Chemical structures of previously identified TYRIs bearing 4-(4-fluorobenzyl) piperazine moiety.

2. Results and discussion

2.1. Investigation into the fundamental interactions between derivative 5b and TyM

Considering as a starting point the best docking pose of compound **5b** in the TyM active site, we calculated all plausible pharmacophore interactions for TyM catalytic pocket by using the tool "*Apo Site Grid*", implemented in the LigandScout software vs 4.3 [14].

The obtained grid (Fig. 2)highlights areas of the binding pocket in which the presence of particular features (i.e. H-bond donor, H-bond acceptor, aromatic ring, hydrophobic groups, negative and positive ionisable groups), would be favourable for the interaction with the target protein. Our focus was especially placed on the aroyl moiety of compound **5b** with the purpose of exploring the wide region in which it is positioned.

As expected, the inhibitor is surrounded by a hydrophobic grid (yellow grid) in the middle and top areas of the cavity (Fig. 2A). Instead, the presence of an aromatic ring (blue grid) seems to be more favorable in the 4-fluorobenzyl zone near the conserved histidines. This evidence reinforces the observation that the introduction of an aromatic moiety is relevant for the stabilization of the inhibitors in the active site through the formation of π-stacking interactions with the catalytic center. A small aromatic zone also appears close to the *o*-tolyl group.

Finally, we have analyzed the grids related to H-bond donor (green grid) or H-bond acceptor (red grid) features. As a result, we found that the insertion of acceptor or donor groups might be favorable on both the aromatic rings of compound **5b** (Fig. 2 B).

Taking into account the obtained pharmacophore grids, we planned the synthesis of a further series of compounds bearing various substituents in *ortho*, *para* and *meta* positions of the phenyl ring. In particular, we selected chlorine and bromine atoms and trifluoromethyl group considering both the hydrophobic

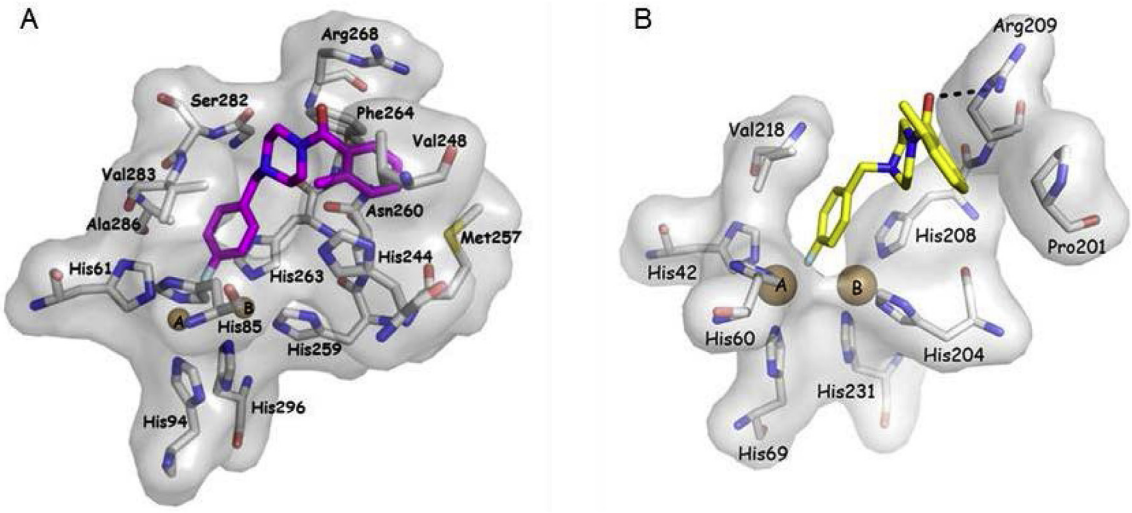

Fig. 1. Comparison of the binding pose of compound **5b** in the catalytic cavities of TyM (A) and TyBm (B). Copper ions are presented as brown spheres, key residues of the pocket are presented as grey sticks and hydrogen bond interactions by dotted lines. The picture was generated using PyMOL (https://pymol.org). (For interpretation of the references to color in this figure legend, the reader is referred to the Web version of this article.)

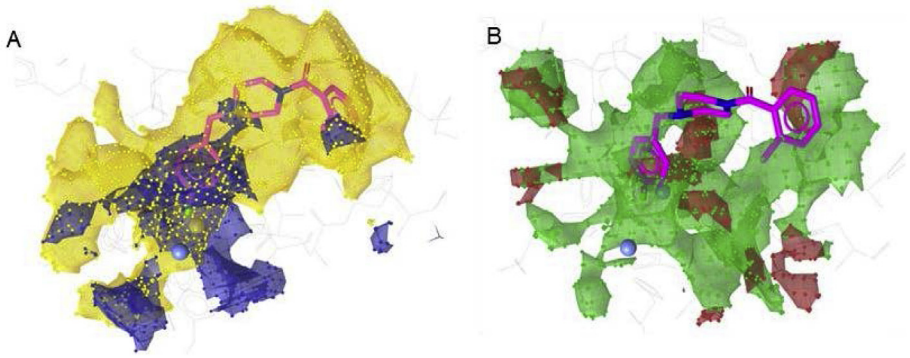

Fig. 2. Apo Site Grid generated starting from the best docking pose of derivative **5b**) in the catalytic site of TyM. A) Yellow grid highlights the favorable presence of hydrophobic groups and specifically blue grid indicates aromatic rings. B) Green grid delineates H-bond donor and red grid H-bond acceptor. The picture was generated using Ligand Scout software [14]. (For interpretation of the references to color in this figure legend, the reader is referred to the Web version of this article.)

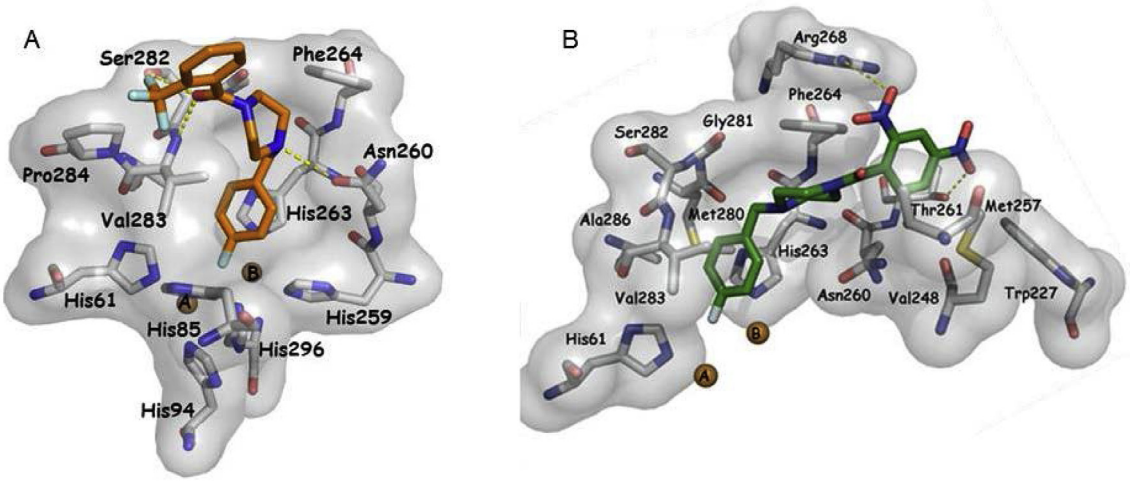

Fig. 3. Plausible binding mode of compounds **13** (A) (orange stick) and **25** (B) (green stick) in the active site of TyM (PDB: 2Y9X). Copper ions are presented as brown spheres, key residues of the pocket are presented as grey sticks and hydrogen bond interactions by dotted lines. The interactions between TyM and inhibitors **13** and **25** were examined using PyMOL and LIGPLUS [16]. All structures presented were generated using PyMOL (https://pymol.org). (For interpretation of the references to color in this figure legend, the reader is referred to the Web version of this article.)

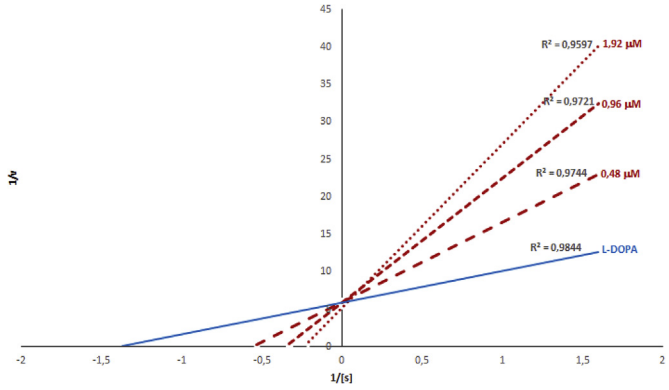

Fig. 4. Lineweaver–Burk plots for the inhibition of tyrosinase using L-DOPA as the substrate in the presence of compound **25**.

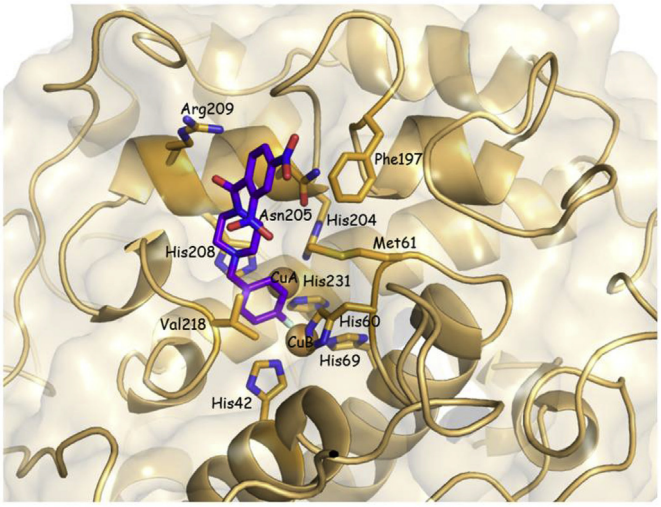

Fig. 5. Structure of compound **25** bound in the active site of tyrosinase from TyBm (PDB: 6QXD). Copper ions are presented as brown spheres and residues surrounding the active site are shown as orange sticks. The structure presented was generated using PyMOL (https://pymol.org). (For interpretation of the references to color in this figure legend, the reader is referred to the Web version of this article.)

interactions (yellow grid) and additional halogen-bond contacts. Moreover, we chose to add nitro, amine and carboxyl groups as H-bond acceptors/donors, as suggested by the red and green grids. Based on previous structure-affinity relationship information [13] we also decided to synthesize several 2,4-disubstituted derivatives.

With the purpose to identify compounds with drug-like properties, we estimated physico-chemical parameters describing pharmaco-kinetic behavior of drugs in the cell environment, i.e. polar surface area, pKa, logP and logD at pH = 7 (https://chemicalize.com/). These parameters were predicted for each designed molecule and are reported in the Supporting Material (Table S1). Furthermore, the presence of pan-assay interference compounds (PAINS) and the conformity to Lipinski's rule were also investigated by means of the free web tool Swiss ADME (http://www.swissadme.ch/). According to the obtained results, all studied compounds displayed good permeability through the biological membranes and no PAINS were detected.

2.2. Chemical synthesis of inhibitors

As depicted in Scheme 1 the new designed 4-(4-fluorobenzyl) piperazine-derivatives **7**–**25** were synthesized by coupling benzoic acids or benzoyl chlorides with 4-(4-fluorobenzyl)piperazine **6** in basic conditions. The 2,4-dihydroxy-derivative **26** was obtained by treating the parent 2,4-dimethoxy analog (**19**) with boron tribromide. Whereas, the amino-derivatives **27**–**30** were prepared by zinc-mediated nitroreduction of parent compounds (**22**–**25**). ^{1}H NMR spectra data of representative compounds are shown in Supporting Material.

2.3. Inhibition of mushroom tyrosinase activity

Tyrosinase inhibitory activity was evaluated for all the synthetized compounds using TyM and L-DOPA as a substrate. The obtained results are summarized in Table 1. Overall, the synthesized compounds showed a good inhibitory activity with IC_{50} values lower or comparable to those of **5b 5a**, and kojic acid (**3**) used as reference compounds. Notably, the collected biological data was coherent with *in silico* results suggested by pharmacophore grids.

It was interesting to note that the introduction of one substituent such as nitro and trifluoromethyl group in *ortho* position of the benzoyl ring allowed us to obtain more active compounds thus reaching IC_{50} values at the nanomolar range for compounds **13** (0.48 μM) and **22** (0.87 μM). The *meta* amino derivative **28** demonstrated inhibitory effects with IC_{50} value of 3.81 μM, whereas the *ortho* and *meta* analogs **27** and **29** possessed activity comparable to those of unsubstituted inhibitor **5a** (13.34 μM) and kojic acid (**3,** 17.76 μM). Concerning the series of 2,4-disubstituted derivatives, the most effective compounds were derivatives **17** (R = 2,4-Cl_2) and **25** (R = 2,4-$(NO_2)_2$) having IC_{50} values of 0.79 and 0.96 μM, respectively.

2.4. Docking into TyM and kinetic studies

With the aim to investigate the binding mode of this series of new designed derivatives we performed docking studies in the active site of TyM from *Agaricus bisporus* retrieved from Protein Data Bank (PDB: 2Y9X) by GOLD software [15]. Fig. 3 displays the best poses found for the most interesting inhibitors **13** (IC_{50} = 0.48 μM) and **25** (IC_{50} = 0.96 μM).

As expected, the two inhibitors are positioned in the TyM active site with the 4-fluorobenzyl moiety placed towards the copper ions and stabilized through π-π interaction with His263. Regarding derivative **13** (Fig. 3A), we found an H-bond interaction between the piperazine nitrogen atom and the carbonyl group of Asn260; moreover, there is a bidentate H-bond interaction between the carbonyl group of the benzamide moiety and the two residues Ser282 and Val283. The trifluoromethyl substituent is oriented in the hydrophobic area lined by residues Pro284 and Val283.

Concerning the docking pose of compound **25** (Fig. 3B), we hypothesized that the nitro group at 2′-position of the benzoyl portion creates a polar contact with Arg268, while the nitro group at 4′-position forms an H-bonding interaction with the side chain of Thr261. Overall, the analysis of the interaction patterns found for the best active inhibitors **13** and **25** confirms that additional interactions mediated by various substituents on the benzoyl portion might justify an improvement of the affinity toward the TyM active site.

Kinetic studies on the diphenolase activity of TyM confirmed the hypothetical binding mode described for compound **25**. Specifically, the inhibitory mechanism was studied by using Lineweaver-Burk double reciprocal plots and the results are displayed in Fig. 4. The Lineweaver-Burk plot demonstrated that V_{max} is the same regardless of concentration of the inhibitor, and K_m increases with increasing concentrations of the inhibitor. This behavior indicates that compound **25** acts as a competitive inhibitor and these

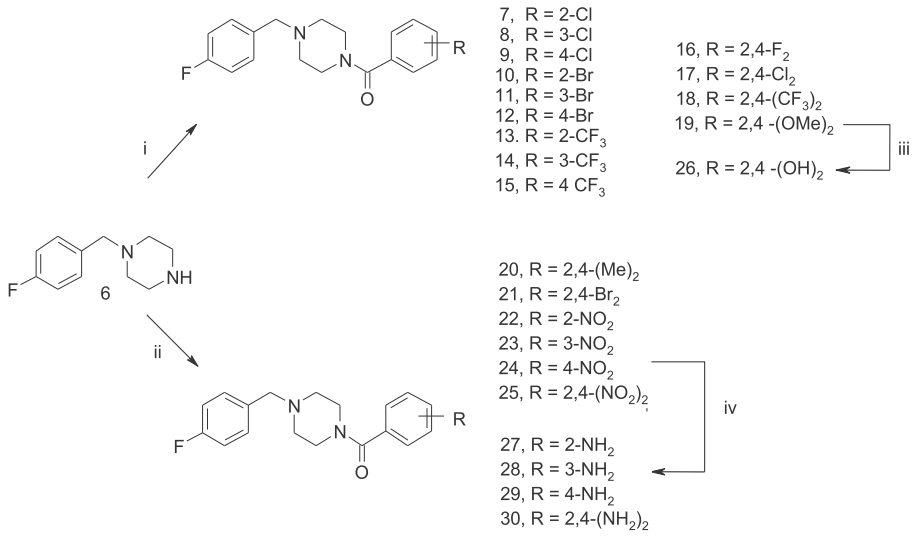

Scheme 1. Reagents and conditions: i) Suitable benzoyl chloride, DCM, EDIPA, MW: 10 min, 50 °C, 200 W; ii) suitable benzoic acid, HBTU, TEA, DMF, rt, 24 h; iii) BBr_3, DCM, 0 °C, rt, 24 h; iv) HCl, Zn, EtOH, reflux, 2 h.

Table 1
Inhibitory activity of derivatives **7**–**30** compared to **5a**, **5b** and kojic acid (**3**) as reference compounds.

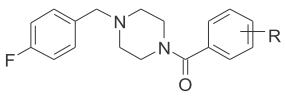

cpd	R	Diphenolase activity IC_{50} (μM)[a]
7	2-Cl	3.12 ± 0.04
8	3-Cl	5.30 ± 0.40
9	4-Cl	3.51 ± 1.24
10	2-Br	2.03 ± 0.05
11	3-Br	2.40 ± 0.28
12	4-Br	4.61 ± 1.83
13	2-CF_3	0.48 ± 0.05
14	3-CF_3	8.43 ± 0.42
15	4-CF_3	3.38 ± 0.07
16	2,4-F_2	1.91 ± 0.13
17	2,4-Cl_2	0.79 ± 0.11
18	2,4-$(CF_3)_2$	1.63 ± 0.11
19	2,4-$(OCH_3)_2$	1.40 ± 0.43
20	2,4-$(CH_3)_2$	3.43 ± 0.08
21	2,4-Br_2	1.05 ± 0.09
22	2-NO_2	0.87 ± 0.08
23	3-NO_2	3.60 ± 0.07
24	4-NO_2	2.05 ± 0.16
25	2,4-$(NO_2)_2$	0.96 ± 0.21
26	2,4-$(OH)_2$	1.49 ± 0.32
27	2-NH_2	10.94 ± 0.44
28	3-NH_2	3.81 ± 0.56
29	4-NH_2	14.66 ± 0.15
30	2,4-$(NH_2)_2$	3.67 ± 0.75
5a	H	13.34 ± 0.73
5b	2-Me	5.25 ± 1.60
Kojic acid, 3		17.76 ± 0.18

[a] IC_{50} values represent the concentration that caused 50% enzyme activity loss. All compounds were studied in a set of experiments performed in three replicates.

findings were in good agreement with our *in silico* studies.

2.5. Crystallographic studies

To get more insight regarding the binding mode of the above reported inhibitors within the active site of TYRs, crystallographic studies were carried out using TyBm. We obtained a crystal structure of TyBm with bound compound **25** in the active site at a resolution of 2.3 Å (Fig. 5) (Table S2 and Fig. S1 as Supplementary Material). The 4-fluorobenzyl moiety of 25 is stabilized by π-π interactions with His208 and is oriented toward CuA at a distance of 1.9 Å, similar to tyrosinase substrates [17] and to the TyM model (Fig. 3B). Furthermore, a polar interaction is observed between Arg209 and the oxygen atom of the carbonyl group in compound 25, similar to compound **5b** as was previously reported (Fig. 1B) [13].

The new synthesized derivatives and in particular compound **25** with positions 2,4-disubstituted with nitro groups, enabled the formation of new interactions in the TyBm active site. These possible intramolecular interactions were calculated using the Arpeggio server, based on geometrical and biochemical features [18]. Compound **25** is further stabilized in the active site by additional π-π interactions observed between the aroyl ring and Phe197. Furthermore, the aroyl ring also interacts with the amide group of Asn205 (Fig. 6A).

Comparing the pose of compound **25** and the starting compound **5b** in the TyBm crystal structure reveals two main differences: (i) While the overall orientation of the 4-fluorobenzyl moiety is similar, this is the first structure of TyBm with a ligand positioned closer and in-between the two copper ions. This outcome is derived from further interactions with surrounding key amino acids in the active site shell, and supports the higher inhibition rate by this compound. (ii) A major movement of Arg209 is observed, which enabled the formation of a hydrogen bond with the carbonyl group, thus stabilizing the bulky compound in the active site (Fig. 6B). The flexibility of Arg209 has been reported beforehand, exhibiting alternative conformations that facilitate the stabilization of ligands in the TyBm binding pocket [19]. It seems that the combination of both the flexibility of the diverse chemical groups in derivatives **7**–**30** and the new interactions in the tyrosinase active site results in a stronger inhibition effect. These data appear coherent with docking results for TyM (see 2.4 section).

2.6. Cell viability

After obtaining encouraging results from the assay experiments, biosafety effectiveness of the promising compound **25** was further

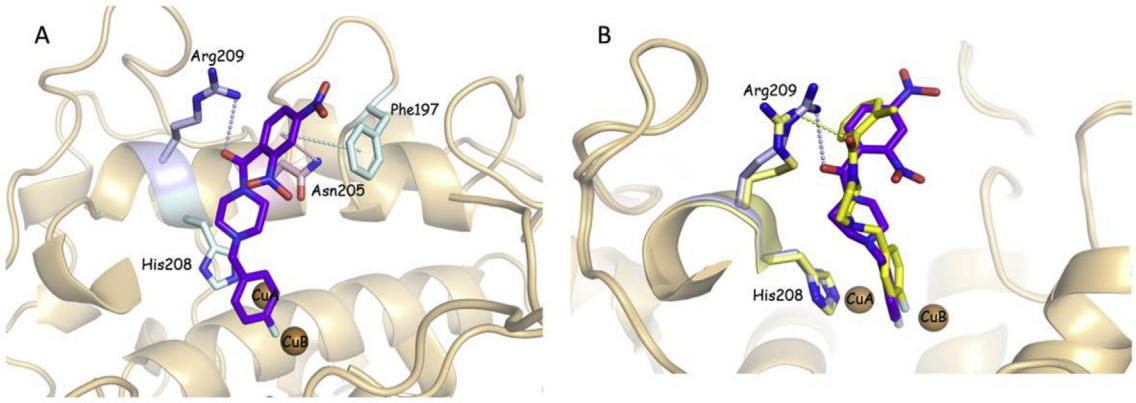

Fig. 6. The 4-(4-fluorobenzyl)piperazin-1-yl](2,4-dinitrophenyl)methanone (**25**) interactions in TyBm active site. A) Compound **25** (purple) is positioned in the active site of TyBm with the oxygen atom of the carbonyl group forming a hydrogen bond with Arg209 (light blue dashed line). π-π interactions with His208 and Phe197 are presented in cyan dashed lines, and amide-ring interaction with Asn205 is presented in a pink dashed line. B) Superposition with TyBm structure binding 4-(4-fluorobenzyl)piperazin-1-yl](2-methylphenyl) methanone (**5b**) (PDB: 6EI4). Compound **5b** (yellow) and **25** (purple) are oriented through hydrophobic interactions with His208. Copper ions (brown) are identical whereas Arg209 is highly flexible. All structures presented were generated using PyMOL (https://pymol.org). (For interpretation of the references to color in this figure legend, the reader is referred to the Web version of this article.)

evaluated. Cells were treated with compound **25** at concentrations ranging from 1 to 100 μM for 48 h at 37 °C and their potential cytotoxic effect on B16F10 cells was determined using the MTT test. Compound **25** exhibited no cytotoxic effect until 10 μM (Fig. 7). As previously reported in literature [20] the reference compound kojic acid (**3**) is not cytotoxic at the same concentrations tested for the compound **25**.

Thus, further experiments using 10 μM of compound concentration were performed.

2.6.1. *Effect on cellular tyrosinase activity and melanin production*

The inhibitory effect of compound **25** on the melanogenesis of B16F10 cells treated with 100 nM α-MSH was examined. In the experiments described here, α-MSH was used as a cAMP inducer to stimulate melanin synthesis. Upon exposure to α-MSH alone, the tyrosinase activity was significantly increased, compared to untreated cells (Fig. 8). After 48 h of incubation with compound **25**, the melanin content of α -MSH-stimulated B16F10 cells was also evaluated.

Fig. 8 shows that compound **25** resulted to be more effective as an anti-melanogenic agent than kojic acid which did not show any inhibition at the same concentration as compared with the control. The results showed that compound **25** inhibited by 22.75 ± 0.48% cellular melanogenesis induced by α-MSH-mediated intracellular cAMP up-regulation.

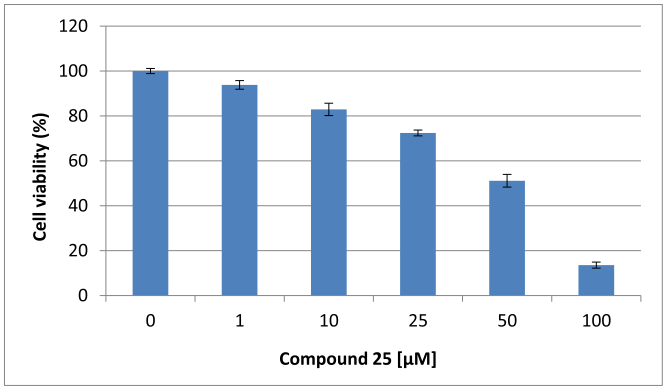

Fig. 7. Effect of compound **25** on B16F10 cell viability. Cells were treated with different concentrations of compound (1–100 μM) and their viability was evaluated by MTT assay. Data represent mean ± SD of triplicate experiments.

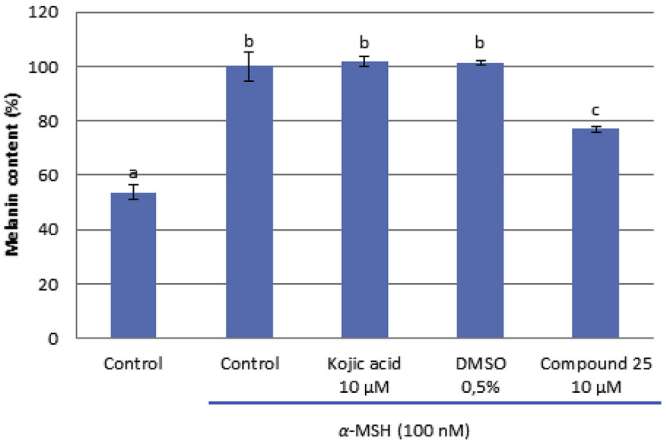

Fig. 8. Effect of compound 25 on B16F10 melanoma cells after incubation for 48 h. Melanin production was expressed as percentage of the control and the effects of extracts were compared with kojic acid as standard inhibitor, and DMSO. Data represent mean ± SD of triplicate experiments. Mean values in the column having different letters are significantly different ($p < 0.05$).

3. Conclusions

In summary, we have investigated the TyM inhibitory effects of twenty-four (4-(4-fluorobenzyl)piperazine derivatives (**7**–**30**) designed on the basis of *in silico* analysis. As result we have found four superior active compounds **13**, **17**, **22** and **25** displaying IC_{50} values at nanomolar concentration as inhibitors using L-DOPA as a substrate. Among these promising molecules, compound **25** (IC_{50} value of 0.96 μM) was nearly 20-fold more active than the positive control kojic acid **3** (IC_{50} 17.76 μM) and revealed to be a competitive inhibitor. Compound **25** also proved to exhibit no considerable cytotoxic effect in B16F10 melanoma cells at the concentration used to determinate the cell melanin production.

Moreover, this compound resulted to be more effective as anti-melanogenic agent when compared with reference compound **3** suggesting a good correlation between mushroom tyrosinase inhibitory properties and melanoma cellular effects. By means of X-

ray and docking studies we demonstrated that compound **25** is able to bind at the catalytic site of tyrosinase for which the 4-fluorobenzyl moiety represents the driving force for the best interaction in the deep region near to copper ions. Moreover, the presence of suitable moieties such as a 2,4-dinitrophenyl group created additional contacts in the top area of the catalytic site thus improving the binding affinity. Overall, these data might be useful to further investigate anti-melanogenic agents from synthetic source structurally related to the best active prototype **25**.

4. Experimental

4.1. Chemistry

All reagents were used without further purification and bought from common commercial suppliers. Microwave-assisted reactions were carried out in a Focused Microwawe TM Synthesis System, Model Discover (CEM Technology Ltd Buckingham, UK). Melting points were determined on a Buchi B-545 apparatus (BUCHI Labortechnik AG Flawil, Switzerland) and are uncorrected. By combustion analysis (C, H, N) carried out on a Carlo Erba Model 1106-Elemental Analyzer we determined the purity of synthesized compounds; the results confirmed a ≥95% purity. Merck Silica Gel 60 F254 plates were used for analytical TLC (Merck KGaA, Darmstadt, Germany). For detection, iodine vapor and UV light (254 nm) were used. Flash Chromatography (FC) was carried out on a Biotage SP1 EXP (Biotage AB Uppsala, Sweden). ^{1}H NMR spectra were measured in dimethylsulfoxide-d6 (DMSO-d_6) or $CDCl_3$ with a Varian Gemini 300 spectrometer (Varian Inc. Palo Alto, California USA); chemical shifts are expressed in δ (ppm) and coupling constants (J) in hertz. All exchangeable protons were confirmed by addition of D_2O. ^{13}C NMR spectra and mass spectra of selected compounds were measured in chloroform ($CDCl_3$) with a Varian and Mass Spectrometer API 2000 respectively.

4.1.1. General procedure for the synthesis of [4-(4-Fluorobenzyl) piperazin-1-yl]methanone derivatives (7–19)

To a solution of 1-(4-fluorobenzyl)piperazine (**6**) (0.5 mmol) in DCM (2 mL) the N,N-diisopropylethylamine (0.75 mmol) and the suitable benzoyl chloride (0.5 mmol) were added. The reaction was carried as previously reported. The final products **7**–**19** were purified by crystallization with Et_2O or by flash chromatography. For compounds **7**–**12, 15, 16** registered CAS numbers have been already assigned. However, their synthetic procedures, chemical properties and structural characterization are not available in literature.

4.1.2. [4-(4-Fluorobenzyl)piperazin-1-yl](2-chlorophenyl) methanone (7)

CAS number: 439847-31-1. Yield 60%. White solid. M.p. 94–95 °C. ^{1}H NMR ($CDCl_3$) (δ): 7.32 (mc, 6H, ArH), 7.00 (mc, 2H, ArH), 3.81 (mc, 2H, CH_2), 3.49 (s, 2H, CH_2), 3.22 (mc, 2H, CH_2), 2.41 (mc, 4H, CH_2). Anal. Calcd for ($C_{18}H_{18}ClFN_2O$): C 65.00, H 5.50, N 8.40. Found: C 65.20, H 5.48, N 8.09.

4.1.3. [4-(4-Fluorobenzyl)piperazin-1-yl](3-chlorophenyl) methanone (8)

CAS number: 423748-71-4. Yield 70%. Oily residue. ^{1}H NMR ($CDCl_3$) (δ): 7.33 (mc, 6H, ArH), 7.01 (mc, 2H, ArH), 3.78 (mc, 2H, CH_2), 3.50 (s, 2H, CH_2), 3.41 (mc, 2H, CH_2), 2.51 (mc, 2H, CH_2), 2.37 (mc, 2H, CH_2). Anal. Calcd for ($C_{18}H_{18}ClFN_2O$): C 65.00, H 5.50, N 8.40. Found: C 65.18, H 5.44, N 8.60.

4.1.4. [4-(4-Fluorobenzyl)piperazin-1-yl](4-chlorophenyl) methanone (9)

CAS number: 945173-43-3. Yield 50%. White solid. M.p. 81–82 °C. ^{1}H NMR ($CDCl_3$) (δ): 7.32 (mc, 6H, ArH), 7.00 (mc, 2H, ArH), 3.82 (mc, 2H, CH_2), 3.49 (s, 2H, CH_2), 3.22 (mc, 2H, CH_2), 2.47 (mc, 4H, CH_2). Anal. Calcd for ($C_{18}H_{18}ClFN_2O$): C 65.00, H 5.50, N 8.40. Found: C 65.15, H 5.59, N 8.44.

4.1.5. [4-(4-Fluorobenzyl)piperazin-1-yl](2-bromophenyl) methanone (10)

CAS number: 1326972-94-4. Yield 50%. White solid. M.p. 86–87 °C. ^{1}H NMR ($CDCl_3$) (δ): 7.56 (mc, 1H, ArH), 7.30 (mc, 5H, ArH), 6.99 (mc, 2H, ArH), 3.82 (mc, 2H, CH_2), 3.49 (s, 2H, CH_2), 3.23 (mc, 2H, CH_2), 2.44 (mc, 4H, CH_2). Anal. Calcd for ($C_{18}H_{18}BrFN_2O$): C 57.30, H 4.80, N 7.40. Found: C 57.21, H 4.75, N 7.44.

4.1.6. [4-(4-Fluorobenzyl)piperazin-1-yl](3-bromophenyl) methanone (11)

CAS number: 439844-72-1. Yield 60%. Oily residue. ^{1}H NMR ($CDCl_3$) (δ): 7.54 (mc, 1H, ArH), 7.28 (mc, 5H, ArH), 7.01 (mc, 2H, ArH), 3.77 (mc, 2H, CH_2), 3.49 (s, 2H, CH_2), 3.40 (mc, 2H, CH_2), 2.51 (mc, 2H, CH_2), 2.37 (mc, 2H, CH_2). Anal. Calcd for ($C_{18}H_{18}BrFN_2O$): C 57.30, H 4.80, N 7.40. Found: C 57.48, H 4.29, N 7.60.

4.1.7. [4-(4-Fluorobenzyl)piperazin-1-yl](4-bromophenyl) methanone (12)

CAS number: 439844-65-2. Yield 55%. White solid. M.p. 87–88 °C. ^{1}H NMR ($CDCl_3$) (δ): 7.53 (mc, 1H, ArH), 7.30 (mc, 5H, ArH), 7.00 (mc, 2H, ArH), 3.76 (mc, 2H, CH_2), 3.49 (s, 2H, CH_2), 3.40 (mc, 2H, CH_2), 2.40 (mc, 4H, CH_2). Anal. Calcd for ($C_{18}H_{18}BrFN_2O$): C 57.30, H 4.80, N 7.40. Found: C 57.25, H 4.88, N 7.30.

4.1.8. [4-(4-Fluorobenzyl)piperazin-1-yl](2-trifluoromethyl) methanone (13)

Yield 90%. Oily residue. ^{1}H NMR ($CDCl_3$) (δ): 7.69 (d, $J = 7.3$ Hz, 1H, ArH), 7.53 (mc, 2H, ArH), 7.28 (mc, 3H, ArH), 6.99 (mc, 2H, ArH), 3.81 (t, $J = 5.0$ Hz, 2H, CH_2), 3.48 (s, 2H, CH_2), 3.16 (t, $J = 5.0$ Hz, 2H, CH_2), 2.50 (mc, 2H, CH_2), 2.29 (mc, 2H, CH_2). Anal. Calcd for ($C_{19}H_{18}F_4N_2O$): C 62.29, H 4.95, N 7.65. Found: C 62.39, H 4.61, N 7.48.

4.1.9. [4-(4-Fluorobenzyl)piperazin-1-yl](3-trifluoromethyl) methanone (14)

Yield 92%. Oily residue. ^{1}H NMR ($CDCl_3$) (δ): 7.67 (mc, 2H, ArH), 7.56 (mc, 2H, ArH), 7.27 (mc, 2H, ArH), 7,00 (mc, 2H, ArH), 3.79 (mc, 2H, CH_2), 3.50 (s, 2H, CH_2), 3.39 (mc, 2H, CH_2), 2.45 (mc, 4H, CH_2). Anal. Calcd for ($C_{19}H_{18}F_4N_2O$): C 62.29, H 4.95, N 7.65. Found: C 62.19, H 4.85, N 7.36.

4.1.10. [4-(4-Fluorobenzyl)piperazin-1-yl](4-trifluoromethyl) methanone (15)

CAS number: 1329056-52-1. Yield 87%. White solid. M.p. 82.8–84.5 °C. ^{1}H NMR ($CDCl_3$) (δ): 7.66 (d, $J = 8.2$ Hz, 2H, ArH), 7.50 (d, $J = 8.2$ Hz, 2H, ArH), 7.27 (mc, 2H, ArH), 7.00 (mc, 2H, ArH), 3.80 (mc, 2H, CH_2), 3.50 (s, 2H, CH_2), 3.37 (mc, 2H, CH_2), 2.44 (mc, 4H, CH_2). Anal. Calcd for ($C_{19}H_{18}F_4N_2O$): C 62.29, H 4.95, N 7.65. Found: C 62.50, H 4.77, N 7.45.

4.1.11. [4-(4-Fluorobenzyl)piperazin-1-yl](2,4-difluorophenyl) methanone (16)

CAS number: 1388318-37-3. Yield 50%. White solid. M.p. 88–90 °C. ^{1}H NMR ($CDCl_3$) (δ): 7.34 (mc, 3H, ArH), 6.91 (mc, 4H, ArH), 3.79 (mc, 2H, CH_2), 3.49 (s, 2H, CH_2), 3.32 (mc, 2H, CH_2), 2.44 (mc, 4H, CH_2). Anal. Calcd for ($C_{18}H_{17}F_3N_2O$): C 64.66, H 5.13, N 8.38. Found: C 64.78, H 5.08, N 8.50.

*4.1.12. [4-(4-Fluorobenzyl)piperazin-1-yl](2,4-dichlorophenyl) methanone **(17)***

Yield 65%. Oily residue. ^{1}H NMR ($CDCl_3$) (δ): 7.41 (mc, 1H, ArH), 7.24 (mc, 4H, ArH), 7.00 (mc, 2H, ArH), 3.80 (mc, 2H, CH_2), 3.49 (s, 2H, CH_2), 3.24 (mc, 2H, CH_2), 2.47 (mc, 3H, CH_2), 2.32 (mc, 1H, CH_2). Anal. Calcd for ($C_{18}H_{17}Cl_2FN_2O$): C 58.87, H 4.67, N 7.63. Found: C 58.90, H 4.44, N 7.78.

*4.1.13. [2,4-Bis(trifluoromethyl)phenyl][4-(4-fluorobenzyl) piperazin-1-yl]methanone **(18)***

Yield 80%. White solid. m.p. 75–77 °C. ^{1}H NMR (DMSO) (δ): 8.13 (mc, 2H, ArH), 7.73 (mc, 1H, ArH), 7.21 (mc, 2H, ArH), 7.12 (m, 2H, ArH), 3.50 (s, 2H, CH_2), 3.69–2.07 (m, 8H, CH_2). ^{13}C NMR (DMSO-d_6) (δ): 164.65 (CO), 162.24 (CF), 160.30 (CF), 138.75, 133.86, 130.70, 128.97, 129.98, 129.74, 126.48, 123.77, 114.80, 60.71, 51.98, 51.65, 46.57, 41.18 Anal. Calcd for ($C_{20}H_{17}F_7N_2O$) C 55.31, H 3.94, N 6.45. Found: C 55.21, H 3.84, N 6.35.

*4.1.14. [4-(4-Fluorobenzyl)piperazin-1-yl](2,4-dimethoxyphenyl) methanone **(19)***

Yield 50%. White solid. M.p. 97–98 °C. ^{1}H NMR ($CDCl_3$) (δ): 7.22 (mc, 3H, ArH), 6.99 (mc, 2H, ArH), 6.46 (mc, 2H, ArH), 3.80 (s, 3H, CH_3), 3.79 (mc, 2H, CH_2), 3.78 (s, 3H, CH_3), 3.47 (s, 2H, CH_2), 3.25 (mc, 2H, CH_2), 2.39 (mc, 4H, CH_2). Anal. Calcd for ($C_{20}H_{23}FN_2O_3$): C 67.00, H 6.50, N 7.80. Found: C 67.15, H 6.42, N 7.73.

*4.1.15. General procedure to synthesize [4-(4-Fluorobenzyl) piperazin-1-yl]methanone derivatives **(20–25)***

A mixture of the suitable carboxylic acid derivative (1 mmol), N,N,N′,N′-tetramethyl-O-(1*H*-benzotriazol-1-yl)uranium hexafluorophosphate (HBTU) (1 mmol, 380 mg) in DMF (4 mL) was stirred at room temperature for 1 h. Then, a solution of the 1-(4-fluorobenzyl)pyperazine (**6**) (1 mmol) in TEA (1 mmol, 140 μL) was added dropwise. The reaction has been accomplished as previously reported [21]. The final compounds **20–25** were purified by crystallization with Et_2O or by flash chromatography. For compounds **23, 24** registered CAS numbers have been already assigned. However, their synthetic procedures, chemical properties and structural characterization are not available in literature.

*4.1.16. [4-(4-Fluorobenzyl)piperazin-1-yl](2,4-dimethylphenyl) methanone **(20)***

Yield 56%. White solid. M.p. 247–249 °C. ^{1}H NMR ($CDCl_3$) (δ): 7.66 (mc, 2H, ArH), 7.13 (t, $J = 8.6$ Hz, 2H, ArH), 7.02 (mc, 3H, ArH), 4.15 (mc, 2H, CH_2), 4.00 (mc, 1H, CH_2), 3.73 (mc, 1H, CH_2), 3.56 (mc, 2H, CH_2), 3.30 (mc, 1H, CH_2), 2.71 (mc, 3H, CH_2), 2.31 (s, 3H, CH_3), 2.23 (s, 3H, CH_3). ^{13}C NMR ($CDCl_3$) (δ): 170.24 (CO), 162.81 (CF), 139.86, 134.45, 133.46, 131.55, 126.80, 116.65, 60.36, 51.31, 21.20, 19.00. MS (ESI): *m/z*: 327.0 [M+H$^+$]. Anal. Calcd for ($C_{20}H_{23}FN_2O$): C 73.59, H 7.10, N 8.58. Found: C 73.40, H 7.28, N 8.40.

*4.1.17. [4-(4-Fluorobenzyl)piperazin-1-yl](2,4-dibromophenyl) methanone **(21)***

Yield 80%. Oily residue. ^{1}H NMR ($CDCl_3$) (δ): 7.73 (mc, 1H, ArH), 7.49 (d, $J = 8.2$ Hz, 1H, ArH), 7.27 (mc, 2H, ArH), 7.12 (d, $J = 8.2$ Hz 1H, ArH), 7.00 (mc, 2H, ArH), 3.80 (t, $J = 5.2$ Hz, 2H, CH_2), 3.50 (s, 2H, CH_2), 3.23 (mc, 2H, CH_2), 2.45 (mc, 3H, CH_2), 2.33 (mc, 1H, CH_2). Anal. Calcd for ($C_{18}H_{17}Br_2FN_2O$): C 47.40, H 3.76, N 6.14. Found: C 47.55, H 3.52, N 6.20.

*4.1.18. [4-(4-Fluorobenzyl)piperazin-1-yl](2-nitrophenyl) methanone **(22)***

Yield 70%. Bright yellow solid. M.p. 101–102 °C. ^{1}H NMR ($CDCl_3$) (δ): 8.18 (d, $J = 7.7$ Hz, 1H, ArH), 7.69 (t, $J = 7.7$ Hz, 1H, ArH), 7.55 (t, $J = 7.7$ Hz, 1H, ArH), 7.38 (d, $J = 7.7$ Hz, 1H, ArH), 7.27 (t, $J = 8.5$ Hz, 2H, ArH), 6.99 (t, $J = 8.5$ Hz, 2H, ArH), 3.83 (mc, 2H, CH_2), 3.49 (s, 2H, CH_2), 3.21 (t, $J = 5.1$ Hz, 2H, CH_2), 2.57 (mc, 2H, CH_2), 2.35 (mc, 2H, CH_2). Anal. Calcd for ($C_{18}H_{18}FN_3O_3$): C 63.00, H 5.30, N 12.20. Found: C 63.33, H 5.28, N 12.31.

*4.1.19. [4-(4-Fluorobenzyl)piperazin-1-yl](3-nitrophenyl) methanone **(23)***

CAS number: 439847-09-3. Yield 76%. Bright yellow solid. M.p. 110–112 °C. ^{1}H NMR ($CDCl_3$) (δ): 8.28 (mc, 1H, ArH), 7.74 (d, $J = 7.4$ Hz, 1H, ArH), 7.62 (mc, 1H, ArH), 7,28 (mc, 3H, ArH), 7.00 (mc, 2H, ArH), 3.80 (mc, 2H, CH_2), 3.51 (s, 2H, CH_2), 3.39 (mc, 2H, CH_2), 2.55 (mc, 2H, CH_2), 2.26 (mc, 2H, CH_2). Anal. Calcd for ($C_{18}H_{18}FN_3O_3$): C 63.00, H 5.30, N 12.20. Found: C 63.10, H 5.24, N 12.01.

*4.1.20. [4-(4-Fluorobenzyl)piperazin-1-yl](4-nitrophenyl) methanone **(24)***

CAS number: 356090-43-2. Yield 80%. Bright yellow solid. M.p. 123–124 °C. ^{1}H NMR ($CDCl_3$) (δ): 8.27 (d, $J = 8.6$ Hz, 2H, ArH), 7.56 (d, $J = 8.6$ Hz, 2H, ArH), 7.27 (t, $J = 8.7$ Hz, 2H, ArH), 7.00 (t, $J = 8.7$ Hz, 2H, ArH), 3.80 (mc, 2H, CH_2), 3.51 (s, 2H, CH_2), 3.36 (mc, 2H, CH_2), 2.53 (mc, 2H, CH_2), 2.37 (mc, 2H, CH_2). Anal. Calcd for ($C_{18}H_{18}FN_3O_3$): C 63.00, H 5.30, N 12.20. Found: C 63.29, H 5.04, N 12.44.

*4.1.21. [4-(4-Fluorobenzyl)piperazin-1-yl](2,4-dinitrophenyl) methanone **(25)***

Yield 62%. Yellow solid. M.p. 169–171 °C. ^{1}H NMR ($CDCl_3$) (δ): 9.01 (s, 1H, ArH), 8.54 (d, $J = 8.3$ Hz, 1H, ArH), 7.61 (d, $J = 8.3$ Hz, 1H, ArH), 7.28 (mc, 2H, ArH), 7.00 (t, $J = 8.7$ Hz, 2H, ArH), 3.84 (mc, 2H, CH_2), 3.52 (s, 2H, CH_2), 3.21 (t, $J = 5.0$ Hz, 2H, CH_2), 2.58 (mc, 2H, CH_2), 2.38 (mc, 2H, CH_2). ^{13}C NMR ($CDCl_3$) (δ): 164.14 (CO), 163.12 (CF), 147.95, 145.74, 138.22, 133.10, 130.50, 129.59, 128.65, 120.44, 115.21, 61.91, 52.11, 46.91. MS (ESI): *m/z*: 388.8 [M+H$^+$]. Anal. Calcd for ($C_{18}H_{17}FN_4O_5$): C 55.67, H 4.41, N 14.43. Found: C 55.59, H 4.30, N 14.15.

*4.1.22. Synthetic procedure for [4-(4-fluorobenzyl)piperazin-1-yl](2,4-dihydroxyphenyl)methanone **(26)***

Compound **26** was synthesized following a previously reported procedure [20]. The final product **26** was purified by treatment with MeOH. Yield 60%. Oily residue. ^{1}H NMR ($CDCl_3$) (δ): 7.27 (t, $J = 8.5$ Hz, 2H, ArH), 7.07 (d, $J = 8.5$ Hz, 1H, ArH), 6.99 (t, $J = 8.5$ Hz, 2H, ArH), 6.37 (mc, 1H, ArH), 6.27 (d, $J = 8.5$ Hz, 1H, ArH), 3.69 (mc, 4H, CH_2), 3.50 (s, 2H, CH_2), 2.48 (mc, 4H, 2 CH_2). Anal. Calcd for ($C_{18}H_{19}FN_2O_3$): C 65.44, H 5.80, N 8.48; Found: C 65.55, H 5.74, N 8.59.

*4.1.23. General procedure to synthesize aminophenyl derivatives **27-30***

Compounds **22–25** were synthesized following a previously reported procedure [22] giving the desired amino-analogues **27–30** through purification with EtOH.

*4.1.24. [4-(4-Fluorobenzyl)piperazin-1-yl](2-aminophenyl) methanone **(27)***

Yield 80%. Oily residue. ^{1}H NMR ($CDCl_3$) (δ): 7.27 (mc, 2H, ArH), 7.14 (mc, 1H, ArH), 7.04 (mc, 3H, ArH), 6.68 (mc, 2H, ArH), 4.31 (bs, 2H, NH_2), 3.62 (mc, 4H, CH_2), 3.48 (s, 2H, CH_2), 2.43 (mc, 4H, CH_2). Anal. Calcd for ($C_{18}H_{20}FN_3O$): C 68.99, H 6.43, N 13.41. Found: C 69.05, H 6.43, N 13.66.

*4.1.25. [4-(4-Fluorobenzyl)piperazin-1-yl](3-aminophenyl) methanone **(28)***

Yield 85%. Oily residue. ^{1}H NMR ($CDCl_3$) (δ): 7.26 (mc, 3H, ArH),

6.99 (mc, 2H, ArH), 6.69 (mc, 3H, ArH), 3.75 (mc, 2H, CH_2), 3.48 (s, 2H, CH_2), 3.43 (mc, 2H, CH_2), 2.45 (mc, 4H, CH_2). Anal. Calcd for ($C_{18}H_{20}FN_3O$): C 68.99, H 6.43, N 13.41. Found: C 69.28, H 6.66, N 13.25.

4.1.26. [4-(4-Fluorobenzyl)piperazin-1-yl](4-aminophenyl) methanone (29)

Yield 80%. White solid. M.p. 146–148 °C. ^{1}H NMR ($CDCl_3$) (δ): 7.27 (mc, 4H, ArH), 7.00 (t, $J = 8.8$ Hz, 2H, ArH), 6.63 (d, $J = 8.8$ Hz, 2H, ArH), 3.85 (mc, 2H, CH_2), 3.62 (mc, 2H, CH_2), 3.48 (s, 2H, CH_2), 2.43 (mc, 4H, CH_2). ^{13}C NMR ($CDCl_3$) (δ): 170.85 (CO), 163.20 (CF), 148.21, 133.57, 130.72, 129.46, 125.36, 115.22, 114.30, 62.27, 53.21. MS (ESI): *m/z*: 314.0 [M+H$^+$]. Anal. Calcd for ($C_{18}H_{20}FN_3O$): C 68.99, H 6.43, N 13.41. Found: C 69.78, H 6.77, N 13.50.

4.1.27. [4-(4-fluorobenzyl)piperazin-1-yl](2,4-diaminophenyl) methanone (30)

Yield 74%. Oily residue. ^{1}H NMR ($CDCl_3$) (δ): 7.25 (mc, 2H, ArH), 7.01 (mc, 2H, ArH), 6.88 (mc, 1H, ArH), 6.00 (mc, 2H, ArH), 3.61 (t, $J = 5.0$ Hz, 4H, CH_2), 3.47 (s, 2H, CH_2), 2.42 (t, $J = 5.0$ Hz, 4H, CH_2). Anal. Calcd for ($C_{18}H_{21}FN_4O$): C 65.84, H 6.45, N 17.06. Found: C 65.44, H 6.30, N 16.88.

4.2. Mushroom tyrosinase inhibition assay

The assay was performed according to the method previously reported [13]. A pre-incubation mixture consisted of samples (0.2–20 μM), L-DOPA (1.25 mM), sodium acetate buffer (0.05 M, pH 6.8) at 25 °C for 10 min. After incubation, mushroom tyrosinase (TyM, 333 U/mL) (EC 1.14.18.1 from Sigma Chemical Company) was added to the mixture. The amount of dopachrome in the reaction mixture was immediately measured as absorbance at 475 nm up to 5 min.

The extent of inhibition, expressed as inhibition percentage, was calculated as follows:

$$Inhibition\ \% = \left(A - \frac{B}{A}\right) x\ 100$$

where A and B represent the absorbance at 475 nm for the blank and sample, respectively. The concentrations leading to 50% activity lost (IC50) were also calculated. Kojic acid was used as a reference standard.

4.3. Kinetic analysis of the tyrosinase inhibition

The reaction mixture consisted of four different concentrations of L-DOPA (0.6–5 mM), the substrate, and TyM in acetate buffer (0.05 M, pH 6.8). Three different concentrations of compound **25** (0.48, 0.96, and 1.92 μM) were added to the reaction mixture. The Michaelis–Menten constant (Km) and maximal velocity (Vmax) of tyrosinase were determined by Lineweaver–Burk plots.

4.4. Computational studies

4.4.1. Generation of pharmacophore-grid

The Apo-Site grids were created by using LigandScout Suite vs 4.3. The docking pose of inhibitor **5b** into TyM active site was employed as starting point for the pharmacophore-grids generation considering the residues within 5 Å from the ligand.

4.4.2. Docking analysis

The crystal structure of Agaricus Bisporus TyM in complex with inhibitor tropolone was retrieved from the RCSB Protein Data Bank (PDB code 2Y9X). The protein and ligands **7**–**30** were prepared by Discovery Studio 2.5.5 [23] and we used all structures to setup docking simulation by Gold 5.0.1 [15]. The above-mentioned procedures are described in detail in previous papers [12,13], the procedures were carried out through slight modifications. Specifically, the side chains of residues His244, Val248, His251, Met257, Asn260, Thr261, Phe264, Arg268 and Leu275 were allowed to rotate according to the internal rotamer libraries in GOLD Suite 5.0.1. The molecular models of the docked compounds were displayed using Pymol software.

4.5. Crystallization and data collection

TyBm crystals were prepared as described previously [17]. Mature crystals were soaked overnight with 1 μL of 10 mM inhibitor 25 dissolved in 100% DMSO and 1 μL of 5 mM CuSO4 in 25% PEG 8K. Data from X-ray diffraction was obtained at the European Synchrotron Radiation Facility (Grenoble, France), at beamline ID 23-1. X-ray diffraction data was indexed, integrated, scaled, and merged using Mosflm and Scala programs [24]. The structure of TyBm in complex with compound 25 was solved using the coordinates of the already determined TyBm structure (PDB 4P6R), and molecular replacement using Phaser [25]. Cycles of refinement were performed using Phenix [26] and Refmac [27,28] along with real-space refinement, manual model building and structure validation using COOT [29]. Information about the collected data, phasing process, and refinement statistics are presented in Table S2 in Supplementary Material.

4.6. Cell line and culture conditions

B16F10 mouse melanoma cells (CRL-6475) were purchased from the American Type Culture Collection (ATCC, Manassas, VA, USA). The cells were cultured in Dulbecco's Modified Eagle Medium (DMEM) supplemented with 10% fetal bovine serum (FBS, Gibco, NY, USA), and 1% penicillin/streptomycin at 37 °C in a humidified atmosphere with 5% CO_2.

4.7. MTT assay for cell viability

The cytotoxic effect of compound **25** was evaluated in B16F10 cells using 3-(4,5-dimethylthiazol-2-yl)-2,5-diphenyltetrazolium bromide (MTT) assay [30]. Briefly, cells were seeded in a 96-well plate ($5x10^3$ cells/well) and incubated at 37 °C with samples at concentration ranging from 1 to 100 μM for 48 h. DMSO was used as solvent for compounds, all activities were performed also in the presence of DMSO alone, as solvent control. After incubation time, cells were labelled with MTT solution for 3 h at 37 °C. The resulting violet formazan precipitates were dissolved in DMSO and color development was measured at 570 nm using a microplate reader (Infinite 200, Tecan, Austria). The absorbance was proportional to the number of viable cells.

4.8. Intracellular melanin content assay

B16F10 cells were grown in 75-cm^2 culture flask at a density 10^5 cells/mL. After 24 h, the medium was substituted by fresh one supplemented with 100 nM α-MSH with 10 μM of compound **25** and incubated for 48 h. Cells treated with 100 nM α-MSH and kojic acid were used as positive control and for comparing the inhibitory strength of the compound. After incubation for 48 h cells were harvested and melanin content in B16F10 cells were measured following a previously described method [31]. Standard curve using synthetic melanin was prepared for each experiment. Intracellular melanin content was calculated by normalizing the melanin value with protein content (μg of melanin/μg of cellular protein) and

expressed as a percentage of the control.

4.9. Statistical analyses

Statistical differences were evaluated using GraphPad Prism software (San Diego, CA, USA). Comparison between groups was assessed by one–way analysis of variance (One–way ANOVA) followed by the Bonferroni Multiple Comparisons Test. The values with $p < 0.05$ were considered significant.

Acknowledgments

This work was supported by the Israel Science Foundation founded by the Israel Academy of Sciences and Humanities, grant number 419/15. We also acknowledge the Russell-Berrie Nanotechnology Institute (RBNI) at the Technion for supporting this research. This research benefited from use of the Technion Center of Structural Biology facility of the Lorry I. Lokey Center for Life Sciences and Engineering. We thank the staff of the European Synchrotron Radiation Facility (beamline ID 23-1) for provision of synchrotron radiation facilities and assistance.

Appendix A. Supplementary data

Supplementary data to this article can be found online at https://doi.org/10.1016/j.ejmech.2019.06.019.

References

[1] A. Sanchez-Ferrer, J.N. Rodriguez-Lopez, F. Garcia-Canovas, F. Garcia-Carmona, Tyrosinase: a comprehensive review of its mechanism, Biochim. Biophys. Acta 1247 (1995) 1–11.
[2] L. Feng, N. Shi, S. Cai, X. Qiao, P. Chu, H. Wang, F. Long, H. Yang, Y. Yang, Y. Wang, H. Yu, De novo molecular design of a novel octapeptide that inhibits in vivo melanogenesis and has great transdermal ability, J. Med. Chem. 61 (2018) 6846–6857.
[3] T. Takizawa, T. Imai, J. Onose, M. Ueda, T. Tamura, K. Mitsumori, K. Izumi, M. Hirose, Enhancement of hepatocarcinogenesis by kojic acid in rat two-stage models after initiation with N-bis(2-hydroxypropyl)nitrosamine or N-diethylnitrosamine, Toxicol. Sci. 81 (2004) 43–49.
[4] M. Nakajima, I. Shinoda, Y. Fukuwatari, H. Hayasawa, Arbutin increases the pigmentation of cultured human melanocytes through mechanisms other than the induction of tyrosinase activity, Pigm. Cell Res. 11 (1998) 12–17.
[5] E.V. Curto, C. Kwong, H. Hermersdorfer, H. Glatt, C. Santis, V. Virador, V.J. Hearing Jr., T.P. Dooley, Inhibitors of mammalian melanocyte tyrosinase: in vitro comparisons of alkyl esters of gentisic acid with other putative inhibitors, Biochem. Pharmacol. 57 (1999) 663–672.
[6] H. Zhou, J.K. Kepa, D. Siegel, S. Miura, Y. Hiraki, D. Ross, Benzene metabolite hydroquinone up-regulates chondromodulin-I and inhibits tube formation in human bone marrow endothelial cells, Mol. Pharmacol. 76 (2009) 579–587.
[7] T. Pillaiyar, V. Namasivayam, M. Manickam, S.H. Jung, Inhibitors of melanogenesis: an updated review, J. Med. Chem. 61 (2018) 7395–7418.
[8] B. Deri, M. Kanteev, M. Goldfeder, D. Lecina, V. Guallar, N. Adir, A. Fishman, The unravelling of the complex pattern of tyrosinase inhibition, Sci. Rep. 6 (2016) 34993.
[9] W.T. Ismaya, H.J. Rozeboom, A. Weijn, J.J. Mes, F. Fusetti, H.J. Wichers, B.W. Dijkstra, Crystal structure of Agaricus bisporus mushroom tyrosinase: identity of the tetramer subunits and interaction with tropolone, Biochemistry 50 (2011) 5477–5486.
[10] A. Bijelic, M. Pretzler, C. Molitor, F. Zekiri, A. Rompel, The structure of a plant tyrosinase from walnut leaves reveals the importance of "Substrate-Guiding residues" for enzymatic specificity, Angew Chem. Int. Ed. Engl. 54 (2015) 14677–14680.
[11] S. Ferro, G. Certo, L. De Luca, M.P. Germano, A. Rapisarda, R. Gitto, Searching for indole derivatives as potential mushroom tyrosinase inhibitors, J. Enzym. Inhib. Med. Chem. 31 (2016) 398–403.
[12] S. Ferro, L. De Luca, M.P. Germano, M.R. Buemi, L. Ielo, G. Certo, M. Kanteev, A. Fishman, A. Rapisarda, R. Gitto, Chemical exploration of 4-(4-fluorobenzyl) piperidine fragment for the development of new tyrosinase inhibitors, Eur. J. Med. Chem. 125 (2017) 992–1001.
[13] S. Ferro, B. Deri, M.P. Germano, R. Gitto, L. Ielo, M.R. Buemi, G. Certo, S. Vittorio, A. Rapisarda, Y. Pazy, A. Fishman, L. De Luca, Targeting tyrosinase: development and structural insights of novel inhibitors bearing arylpiperidine and arylpiperazine fragments, J. Med. Chem. 61 (2018) 3908–3917.
[14] G. Wolber, T. Langer, LigandScout: 3-D pharmacophores derived from protein-bound ligands and their use as virtual screening filters, J. Chem. Inf. Model. 45 (2005) 160–169.
[15] G. Jones, P. Willett, R.C. Glen, A.R. Leach, R. Taylor, Development and validation of a genetic algorithm for flexible docking, J. Mol. Biol. 267 (1997) 727–748.
[16] R.A. Laskowski, M.B. Swindells, LigPlot+: multiple ligand-protein interaction diagrams for drug discovery, J. Chem. Inf. Model. 51 (2011) 2778–2786.
[17] M. Goldfeder, M. Kanteev, S. Isaschar-Ovdat, N. Adir, A. Fishman, Determination of tyrosinase substrate-binding modes reveals mechanistic differences between type-3 copper proteins, Nat. Commun. 5 (2014) 4505.
[18] H.C. Jubb, A.P. Higueruelo, B. Ochoa-Montano, W.R. Pitt, D.B. Ascher, T.L. Blundell, Arpeggio: a web server for calculating and visualising interatomic interactions in protein structures, J. Mol. Biol. 429 (2017) 365–371.
[19] M. Goldfeder, M. Egozy, V. Shuster Ben-Yosef, N. Adir, A. Fishman, Changes in tyrosinase specificity by ionic liquids and sodium dodecyl sulfate, Appl. Microbiol. Biotechnol. 97 (2013) 1953–1961.
[20] M.J. Chen, C.C. Hung, Y.R. Chen, S.T. Lai, C.F. Chan, Novel synthetic kojic acid-methimazole derivatives inhibit mushroom tyrosinase and melanogenesis, J. Biosci. Bioeng. 122 (2016) 666–672.
[21] E. Bruno, M.R. Buemi, A. Di Fiore, L. De Luca, S. Ferro, A. Angeli, R. Cirilli, D. Sadutto, V. Alterio, S.M. Monti, C.T. Supuran, G. De Simone, R. Gitto, Probing molecular interactions between human carbonic anhydrases (hCAs) and a novel class of benzenesulfonamides, J. Med. Chem. 60 (2017) 4316–4326.
[22] S. Ferro, M.R. Buemi, L. De Luca, F.E. Agharbaoui, C. Pannecouque, A.M. Monforte, Searching for novel N-1-substituted benzimidazol-2-ones as non-nucleoside HIV-1 RT inhibitors, Bioorg. Med. Chem. 25 (2017) 3861–3870.
[23] Discovery Studio 2.5.5 Accelrys, 2009. San Diego, CA, http://www.accelrys.com.
[24] A.G.W. Leslie, Joint CCP4+ ESF-EAMCB Newsletter on Protein Crystallography, vol. 26, 1992.
[25] A.J. McCoy, Solving structures of protein complexes by molecular replacement with Phaser, Acta Crystallogr D Biol Crystallogr 63 (2007) 32–41.
[26] P.D. Adams, P.V. Afonine, G. Bunkoczi, V.B. Chen, I.W. Davis, N. Echols, J.J. Headd, L.W. Hung, G.J. Kapral, R.W. Grosse-Kunstleve, A.J. McCoy, N.W. Moriarty, R. Oeffner, R.J. Read, D.C. Richardson, J.S. Richardson, T.C. Terwilliger, P.H. Zwart, PHENIX: a comprehensive Python-based system for macromolecular structure solution, Acta Crystallogr D Biol Crystallogr 66 (2010) 213–221.
[27] G.N. Murshudov, A.A. Vagin, E.J. Dodson, Refinement of macromolecular structures by the maximum-likelihood method, Acta Crystallogr D Biol Crystallogr 53 (1997) 240–255.
[28] P. Skubak, G.N. Murshudov, N.S. Pannu, Direct incorporation of experimental phase information in model refinement, Acta Crystallogr D Biol Crystallogr 60 (2004) 2196–2201.
[29] P. Emsley, K. Cowtan, Coot: model-building tools for molecular graphics, Acta Crystallogr D Biol Crystallogr 60 (2004) 2126–2132.
[30] T. Mosmann, Rapid colorimetric assay for cellular growth and survival: application to proliferation and cytotoxicity assays, J. Immunol. Methods 65 (1983) 55–63.
[31] F. Pintus, M.J. Matos, S. Vilar, G. Hripcsak, C. Varela, E. Uriarte, L. Santana, F. Borges, R. Medda, A. Di Petrillo, B. Era, A. Fais, New insights into highly potent tyrosinase inhibitors based on 3-heteroarylcoumarins: anti-melanogenesis and antioxidant activities, and computational molecular modeling studies, Bioorg. Med. Chem. 25 (2017) 1687–1695.